Age-associated changes in human circadian rhythms

by

Michelle Sun

BS Biological Sciences, Carnegie Mellon University, 2021

Submitted to the Graduate Faculty of the

School of Public Health in partial fulfillment

of the requirements for the degree of

Master of Science in Biostatistics

University of Pittsburgh

2024

UNIVERSITY OF PITTSBURGH

SCHOOL OF PUBLIC HEALTH

This thesis was presented

by

Michelle Sun

It was defended on

April 10, 2024

and approved by

Jiebiao Wang, PhD, Assistant Professor, Biostatistics
School of Public Health, University of Pittsburgh

George Tseng, ScD, Professor and Vice Chair for Research, Biostatistics
School of Public Health, University of Pittsburgh

Bokai Zhu, PhD, Assistant Professor, Division of Endocrinology and Metabolism
School of Medicine, University of Pittsburgh

Thesis Advisor: Jiebiao Wang, PhD, Assistant Professor, Biostatistics
School of Public Health, University of Pittsburgh

Age-associated changes in human circadian rhythms

Michelle Sun, MS

University of Pittsburgh, 2024

Cellular circadian clocks support homeostasis by synchronizing essential biological processes to the external day-night cycle. Emerging evidence has demonstrated that the functionality of these clocks changes with age. We leverage data from the Genotype-Tissue Expression project (GTEx) to examine age-dependent changes in rhythmic gene expression programs across 4 human tissues: lung, heart, skeletal muscle, and adrenal gland. Our analysis reveals a shift in the age-related timing of gene expression peaks, transitioning from tissue-specific clustering to a broad categorization at dawn and dusk. We observe a decline in the rhythmicity of genes associated with cell growth and differentiation, paralleled by an increase in the rhythmic expression of genes linked to mitochondrial respiration. We find that the inferred circadian clock outputs are highly dependent on the methodological approach—ordering donors by time-of-death or utilizing circadian phase estimation algorithms leads to different interpretations of the data. Our findings offer insights into the aging transcriptional landscape in humans and highlight the influence of methodology in human circadian rhythm research, providing direction for future studies.

Public Health Significance: Understanding how circadian function changes with age can contribute to strategies aimed at promoting healthy aging, potentially extending the health span and improving quality of life for older adults.

Table of Contents

List of Tables

List of Figures

Preface

To my thesis advisors, professors, and cohort, thank you for your confidence in me through this process.

To Dr. Jiebiao Wang, thank you for generously and patiently giving me the freedom to experiment, and for asking the right questions to push me forward.

To Dr. George Tseng, thank you for your expertise and your insightful advice.

To Dr. Bokai Zhu, thank you for being a constant bright reminder of how much fun it is to be a scientist and to love what you do.

To my loved ones, thank you for giving me a reason to stop working and to enjoy all the other wonderful things the world has to offer.

1.0 Introduction

The life of most organisms is influenced by two biological processes: biological rhythms and the biology of aging.

Biological rhythms include any recurrent molecular, physiological, or behavioral process that cycles without any geophysical cues. Such rhythms are synchronized to environmental signals called *zeitgebers* which enable coordination between rhythmic processes and the time of day or year (Touitou et al., 1992). This allows organisms to anticipate environmental changes and internal needs, enhancing survival and function (Moore-Ede et al., 1986).

The circadian system is a biological rhythm with a period of 24 hours. The central clock of the circadian system is the suprachiasmatic nucleus (SCN) of the hypothalamus, which receives daily light input to synchronize the circadian oscillations of gene expression in every tissue and cell type. While the SCN imprints a whole-body circadian rhythmicity, this central clock works in parallel with autonomously regulated circadian clocks in each tissue, known as peripheral clocks. The SCN and peripheral tissues all share a similar molecular clock mechanism comprised of transcription-translation feedback loops between the core clock genes. Key core clock genes include transcriptional activators BMAL1 and CLOCK, and their negative regulators PER and CRY. These core clock genes regulate the expression of numerous clock-controlled genes, impacting tissue-specific activities (Takahashi et al., 2017).

The functionality of these rhythms, however, diminishes with age. Studies have shown that with age, there are reduced amplitudes and increased scatter in circadian phases, and disrupted cell and tissue synchronization (Hu et al., 2009; Farajnia et al., 2012). This manifests in age-related declines in circadian behavior such as changes in sleep/wake activity, body temperature, hormone

release (Hood and Amir, 2017). Aging is also associated with a higher mortality following repeated changes to light/dark cycle, also known as "jetlag" (Inokawa et al., 2020). Recently, Wolff et al. (2023) obtained a systems level understanding of the aging circadian transcriptome in mice. They carried out a 48-hr circadian transcriptomic analysis in young and old mice across multiple tissues. From their results, they suggested that age-associated changes in circadian clock output led to reduced predictive homeostasis, likely contributing to the frailty and diminished resilience in the old. They further posit that this loss in predictive rhythmic pathways is compensated for by increased reactive pathways in response to stressors. For example, in mouse muscle tissue, the loss of rhythmic autophagic processes with age is compensated for by a general overexpression of autophagy genes in the old during the active phase.

Our goal is to perform a comparative analysis using human data. Using transcriptomic data from the Genotype-Tissue Expression project (GTEx), we detect rhythmically expressed genes between two age groups within four tissues: heart, lung, muscle, and adrenal gland tissue.

In order to reconstruct molecular rhythmicity, the tissue samples are ordered based on the time of death (TOD) of the donors. Although this is common practice in previous rhythm studies in postmortem human tissue (Chen et al., 2016; Li et al., 2013; Scott et al., 2023), there are concerns over discrepancies between actual and annotated TOD, RNA degradation due to postmortem delay, and varying chronotypes between individuals. (Zhu et al., 2017; Roenneberg et al., 2007). To address these concerns, Talamanca et al. (2023) combined GTEx transcriptomes with an algorithm that estimates the circadian phase of donors.

We compare our results with that of Talamanca et al. and Wolff et al. By doing so, we define the age-related changes in human circadian clock output, as well as assess whether novel

phase estimation algorithms can help human circadian studies capture findings found in controlled mouse time course studies.

2.0 Methods

2.1 Data

2.1.1 Data source

Data was retrieved from the Genotype-Tissue Expression (GTEx) project. Gene mRNA read count data for skeletal muscle, lung, adrenal medulla, and left ventricle heart tissue was downloaded from GTEx V8 (2017-06-05_v8_RNASeQCv1.1.9). Access to complete donor phenotype and sample annotations was obtained from dbGaP.

2.1.2 Data cleaning and processing

Tissue samples were removed from the study if the donor's time of death (TOD) was unavailable or if they had a death classification of "intermediate" or "slow" death under the 4-point Hardy Scale. To control sample quality, we selected samples with an RNA integrity number (RIN) of 6 or greater, and an ischemic time under 24 hours. We classified tissue samples based on the donor's age as younger (<=45 y) or older (>= 60 y). Not all tissues were collected for each donor, and so the final sample size varied across tissues.

Time of Death Analysis in the Zeitgeber Timescale

The TOD for each subject was normalized to the zeitgeber time (ZT) scale. For each subject, TOD was noted down to the exact hour and minute, and the season, but did not include

exact date or location. The location was approximated as Philadelphia, PA seeing as it is the largest GTEx project donor source site (NIH, 2010). The date was approximated based on the season: December 1st for winter; October 1st for fall; April 1st for spring; and July 1st for summer. The sunrise time was calculated based on these approximate dates and locations. Subject's TOD was set as ZT = t hours after sunrise.

RNA-seq Data Processing

The raw count data was normalized to counts per millions of reads (CPM), then underwent log2 transformation with a pseudo-count of 1 to avoid log2(0). For each tissue, genes with mean log2(cpm+1) < 1 were removed to control for false positives. For rhythmicity analysis, the log-transformed CPM normalized data (LCPM) was quantile normalized for each tissue using the preprocessCore package.

A principal component analysis (PCA) was performed on the LCPM data for each tissue. To see which covariates explained the variation in the first 2 principal components, linear regression models were fitted using the lm() function. Covariates of interest included ischemic time, Hardy death classification, sex, age, and tissue-specific morbidities (i.e. cardiovascular disease in heart tissue). Model selection was performed using bidirectional stepwise AIC (Akaike Information Criterion) to choose the most parsimonious model. Based on the results, we regressed out ischemic time, and Hardy death classification with a linear regression model on the LCPM data. This was done for each gene in each tissue. The residuals of these fits were used for downstream rhythmicity analyses.

2.2 Statistical analysis

2.2.1 DiffCircaPipeline rhythmicity analysis

We employed the DiffCircaPipeline software (Xue et al., 2023) to perform Cosinor model fitting and comparison for each tissue. The Cosinor model assumes a sinusoidal relationship between gene expression and ZT. It is defined as (Cornelissan 2014):

$$Y_i = A\cos\left(\frac{2\pi}{P}(t_i - \phi)\right) + M + \varepsilon_i \ ,$$

where $i\ (1 \le i \le n)$ is the sample index; n is the number of samples in each age group for each tissue; Y_i is the quantile normalized LCPM values for genes in sample i; t_i is the ZT for sample i ; A is the amplitude; M is the midline estimating statistic of rhythm (MESOR);ϕ is the phase; P is the period, fixed at 24 h for circadian rhythms; and ϵ_i is a normally distributed error term.

Using the trigonometric conversion $\cos(x + y) = \cos x \cos y - \sin x \sin y$, the previous equation can be rewritten as:

$$Y_i = \beta_1 \cos(\omega t_i) + \beta_2 \sin(\omega t_i) + M + \varepsilon_i \ ,$$

In which $\beta_1 = A\cos(\omega\phi)$, $\beta_2 = A\sin(\omega\phi)$, and $\omega = \frac{2\pi}{P}$. Estimates for β_1 and β_2 are derived using ordinary least squares regression, which is then used to calculate the rhythm parameters A and ϕ.

A gene is determined to be significantly rhythmic based on an F-test. The F-statistic compares the model sum of squares (MSS) to the residual sum of squares (RSS):

$$F = \frac{MSS/2}{RSS/(N-3)} \ \sim \ F(2, N-3)$$

where 2 represents the degrees of freedom associated with the model, and N-3 is the degrees of freedom associated with the error term (number of observations minus number of parameters). $RSS = \sum_{i=1}^{n} \left(Y(t_i) - \hat{Y}(t_i)\right)^2$ and $MSS = \sum_{i=1}^{n} \left(\hat{Y}(t_i) - \overline{Y}(t_i)\right)^2$ where $\hat{Y}(t_i)$ are the predicted values and $\overline{Y}(t_i)$ is the mean of the observed data.

We test the hypotheses $H_0: A = 0$ and $H_A: A \neq 0$. When $A = 0$, Y_i is not determined by t_i. Thus, the null hypothesis is rejected when $F > F_{1-\alpha,2,N-3}$. For this analysis, α is set to 0.05.

After rhythmically expressed genes (REGs) are identified separately for each age group, they are categorized by type of rhythmicity: arrhythmic, rhythmic in the younger group, rhythmic in the older group, and rhythmic in both. This is done using a selective sequential model selection (SSMS) procedure to control false positives (identifying genes as within a rhythmic group when they are not). This algorithm involves a nested model path, starting with the simplest model (arrhythmic) to more complex models (rhythmic in one group, followed by rhythmic in both):

P-values are calculated by likelihood ratio testing between models on the path. The selected model is decided by a Sidak ForwardStop rule where the step we stop at, k, is determined by the p-values of previous steps in relation to the significance level:

$$\hat{k} = \max\left\{k: \frac{1}{k}\sum_{i=1}^{k} \log(1 - p_i) \leq \alpha\right\}.$$

2.2.2 CHIRAL-based rhythmicity analysis

Circular HIerarchical Reconstruction Algorithm (CHIRAL) is an algorithm developed by Talamenca et al. (2023) for the purpose of assigning donors a phase along the circadian clock. The

algorithm involves modeling the LCPM matrix (E_{gc}) of each tissue with a multivariate harmonic regression model:

$$E_{gc} = \mu_g + a_g cos(\phi_c) + b_g \sin(\phi_c) + \epsilon,$$

in which g refers to gene, c refers to condition (sample), ϵ is a normally distributed error term, a_g and b_g are gene Fourier parameters (close to zero if genes are non-rhythmic), and ϕ_c are the unknown sample phases.

The process of estimating unknown sample phases is unsupervised in nature. It begins by selecting clock reference genes (CRGs). In this case, the CRGs used were: DBP, PER3, TEF, NR1D2, PER1, PER2, NPAS2, ARNTL, NR1D1, CRY1, CRY2, CIART. Model inputs are the LCPM matrix of CRGs for each sample and Gaussian distributed priors over the gene parameters. A Bayesian calculation marginalizes over the gene parameters distribution to derive posterior distributions over ϕ_c .The maximum a posteriori estimators are inferred using an expectation maximization (EM) procedure. This algorithm iterates between two steps. The expectation (E) step uses current estimates to evaluate the "Q function", a function for the expected log likelihood. Then the maximization (M) step computes parameters which maximizes the Q function. These estimated parameters are then fed back into the E step.

During the EM procedures, cosine and sine vectors are constrained to a norm of 1. CRGs are weighted based on their rhythmicity, and therefore their informativeness.

ϕ_c refers to tissue sample phases. These are combined in ϕ_{td} , a set of tissue (t) phases for each donor (d). The donor phases (ϕ_d) are then calculated based on the assumption that $\phi_d = \phi_{td} + \delta\phi_t$, where $\delta\phi_t$ is the tissue specific shift in phase that is shared among all donors. Because of this assumption, individual deviations from the population mean are ignored.

Talamanca et al. did report that majority of tissues were similarly phased, and outliers were tissues with weak clocks. Therefore, these tissues were weighted less when assigning ϕ_d.

After phase estimation, rhythmic genes were detected with multivariate harmonic regression by inputting the LCPM matrix of all genes:

$$E_{gd} = \mu_g + a_g cos(\phi_d) + b_g \sin(\phi_d) + \epsilon.$$

A gene was determined to be significantly rhythmic using a likelihood ratio test in which $H_0: a_g = b_g = 0$. P-values were computed from a chi-squared distribution and adjusted with Benjamini-Hochberg (BH) correction.

2.2.3 Differential expression analysis

The TODs were categorized into 4-time domains defined as Active Phase: ZTs (4-10], Activity Offset Phase: ZTs (10-16], Rest Phase: ZTs (16-22], and Activity Onset Phase: ZTs (22-4]. Within each time domain and for each tissue, the DESeq2 R package was utilized to identify genes showing increasing/decreasing expression values between age groups. The DESeq2 method uses a model based on the negative binomial distribution to account for variability in gene count data. The Wald test was used to assess the significance of estimated log2 fold changes and the false discovery rate was controlled for using BH correction.

Rank-rank hypergeometric overlap (RRHO) was utilized to compare the differential expression (DE) patterns between our GTEx analysis and published mouse results from Wolff et al. (2023). RRHO was performed using the RRHO2 package (Cahill, 2018). This approach performs "threshold-free" comparisons because significance cut-offs may miss concordantly expressed genes. We inputted the full gene list from our GTEx analysis, regardless of p-value, against Wolff et al.'s DE list at a cutoff of q-value > 0.05. Genes were ranked by p-value and log2

fold change. For each ranked gene, a significance value was calculated via a hyper-geometric distribution which represented the significance of the number of overlapping genes. A chi-squared test was performed to identify whether the proportion in the number of concordant/discordant genes was significant (p-value < 0.05).

2.2.4 GO pathway enrichment

The functional annotations of REGs (p-value < 0.03) and DEGs (q-value < 0.1) were examined using the clusterProfiler package in R. Specifically, the *enrichGO* function calculated statistically significant enrichment for gene ontology (GO) terms. This function is based on a hypergeometric distribution to check whether the number of selected genes that fall into a specific GO term is higher than what would be expected by chance. Multiple comparison correction was performed using the Benjamini-Hochberg method. Redundant pathways were filtered out using REVIGO.

3.0 Results

This study examined the human circadian transcriptome utilizing samples from the GTEx (v8) project. RNA-seq data was analyzed from four tissues: lung, skeletal muscle, heart left ventricle, and adrenal medulla. These tissues were selected because Wolff et al. detailed the age-related circadian changes of these tissues in male mice. This gives an opportunity to compare mouse results to human results. Wolff et al. also examined hypothalamus and kidney tissue, but it was not included here because we aimed for a sample size of at least 50 donors after stratifying subjects into Young (≤45 y) and Old (≥60 y) groups. The final sample sizes are shown in Table 1.

Table 1: Demographics

Tissue	Age Group	N	Age (mean years (sd))	Sex = Male (%)
Lung	Young	98	34.1 (7.2)	67%
	Old	136	64.8 (3.2)	68%
Muscle	Young	176	33.3 (7.8)	66%
	Old	194	64.8 (3.2)	72%
Heart	Young	68	34.6 (8)	56%
	Old	103	64.5 (3)	70%
Adrenal	Young	62	35.1 (7.7)	60%
	Old	59	64.6 (3.1)	56%

3.1 Circadian transcriptome analysis using TOD and DiffCircaPipeline

Within each tissue, gene expression data was corrected for sample covariates to reduce variability not related to age or circadian oscillations. Samples were ordered by the donor's time of death (TOD). The corrected and ordered data was then fitted to sinusoidal regression models with a period of 24 hr using the DiffCircaPipeline package (Xue et al., 2023). Rhythmically expressed genes (REGs) were defined based on a raw p-value < 0.03. The sequential series model selection (SSMS) procedure, also offered through DiffCircaPipeline, was implemented to categorize REGs into four types of rhythmicity: (i) only rhythmic in the older group; (ii) only rhythmic in the younger group; (iii) rhythmic in both groups; (iv) arrhythmic.

Across all tissues except the heart, we found that the number of REGs increased by an average of 48% with age. In the lung, there were 248 REGs in Young and 486 in Old (Figure 1A). In muscle, there were 287 REGs in Young and 574 REGs in Old (Figure 1B). In the adrenal gland, 241 REGs were identified in Young and 550 REGs in Old (Figure 1D). Only the heart showed little difference with 333 REGs in Young and 335 REGs in Old (Figure 1C). The majority of REGs were age-specific with only 2%- 5% of REGs conserved between age groups. Wolff et al. found that in mice, the number of REGs tended to decrease with age, and that over 90% of REGs were age specific.

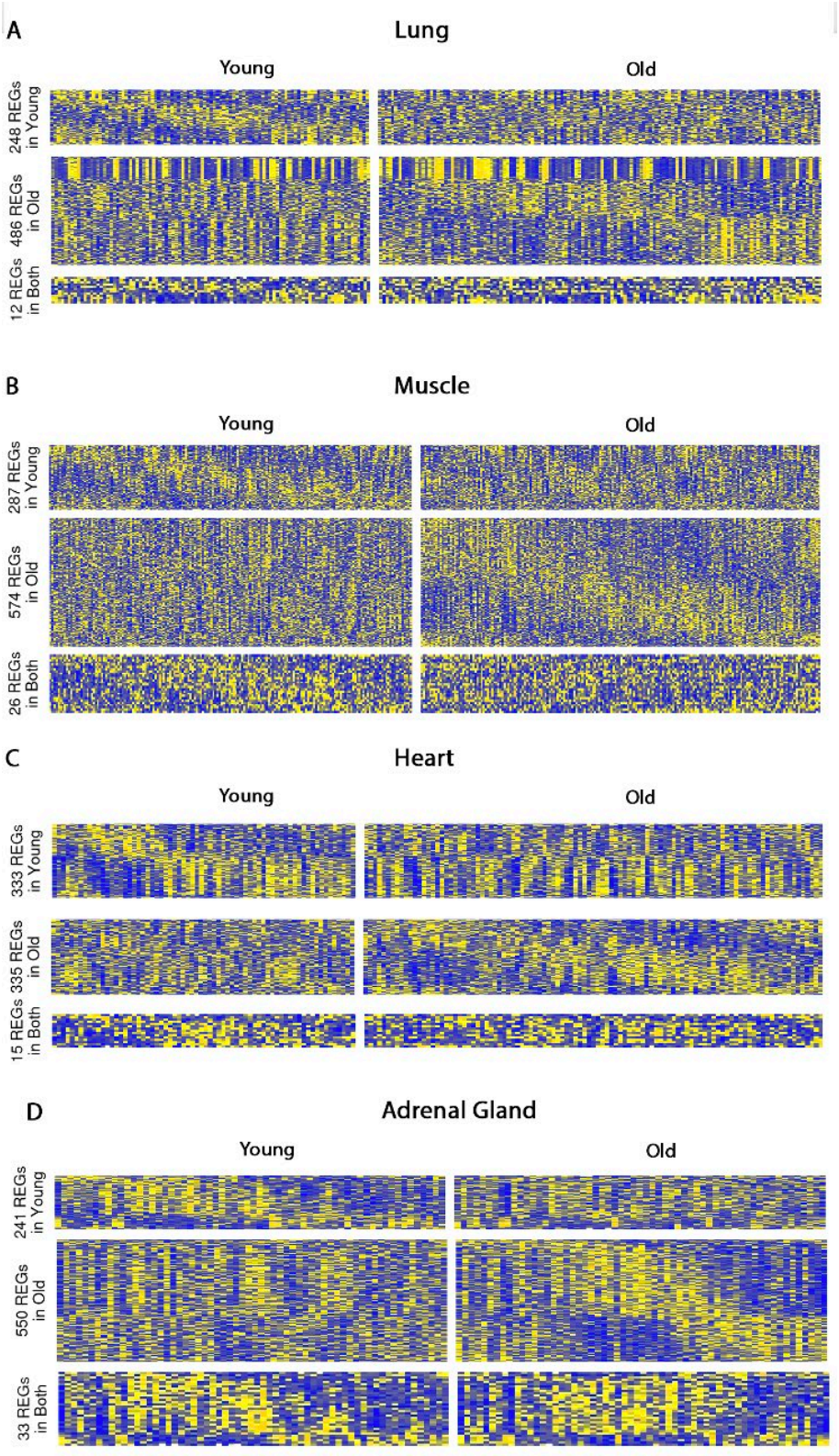

Figure 1: Heatmap of rhythmically expressed genes (REGs)

The majority of identified REGs were tissue-specific, with only five genes shared across all tissues in the older group: *PER3, CIART, PER2, NR1D2,* and *ARNTL*. These genes are considered core clock genes (CCGs) which serve as the main output and regulators of the circadian clock (Cox, 2019). Their multi-tissue conservation is consistent with Wolff et al. and previous multi-organ mouse studies (Zhang et al., 2014). Unexpectedly, no genes were shared across all tissues in the younger group. Additionally, in all tissues except lung, the core clock genes were dampened in Young compared to Old. This contradicts Wolff et al.'s results and a previous study looking at age-dependent circadian changes in the human postmortem brain (Chen et al., 2016).

3.2 Comparison of TOD and CHIRAL based analyses

Our rhythmicity analysis shows contrary findings to Wolff et al. in terms of the number of REGs and the expression of core clock genes with age. We wondered if this was due to using TOD to order subjects and reconstruct molecular rhythmicity. Therefore, we compared our results and Wolff et al's mouse timecourse results to that of Talamenca et al. (2023). In their recent study, Talamanca et al. also looked at age-dependent changes in circadian rhythms in humans. Notably, they combined GTEx transcriptomes with CHIRAL, an algorithm they developed to assign circadian phase to human donors using a set of weighted clock reference genes. Their age groups were defined similarly as Young (<50 y) and Old (>60 y).

Figure 2 shows the difference in the number of REGs identified. To define rhythmicity, Wolff et al. used a raw p-value < 0.01 and Talamanca et al. used a q-value < 0.2. In lung and heart tissue, CHIRAL analysis showed a 22% and 55% age-related decrease in the number of REGs

respectively. In muscle and adrenal gland tissue, CHIRAL analysis showed a 4.5% and 10% increase in the number of REGs respectively.

Table 2 shows the age-related change in amplitude of 16 CCGs. The CHIRAL analysis found no change in the amplitude of most CCGs with age.

Figure 2: Number of REGs identified across methods

Table 2: Change in amplitude of core clock genes (CCGs) with age

Blue-shaded cells indicate CCGs that decrease in amplitude with age. Yellow indicates an increase in amplitude and gray indicates no change in amplitude.

	Mouse				TOD				CHIRAL			
	Lung	Muscle	Heart	Adrenal	Lung	Muscle	Heart	Adrenal	Lung	Muscle	Heart	Adrenal
Arntl	-6.079	1.912	-4.680	-15.253	0.131	0.435	0.574	0.021	0.000	0.000	0.000	0.000
Bhlhe40	0.983	22.093	1.845	25.787	0.091	0.055	0.167	0.139	0.000	0.000	0.000	0.000
Bhlhe41	0.758	3.929	-3.358	0.827	0.077	0.126	0.020	0.138	-0.661	0.000	0.000	0.000
Ciart	-4.123	-2.031	-2.178	-0.480	-0.257	0.295	0.331	0.199	0.133	0.518	0.000	0.557
Clock	-13.895	7.716	-0.917	-2.915	0.012	0.058	0.010	-0.009	-0.136	0.000	0.000	0.000
Cry1	-2.884	-3.519	0.787	-7.758	-0.029	0.166	0.130	-0.083	-0.552	0.000	0.000	0.000
Cry2	-11.962	4.207	-3.899	1.041	-0.135	0.031	-0.022	-0.006	0.166	0.286	0.000	0.000
Dbp	-40.725	-17.032	-31.690	-2.650	-0.323	0.407	0.288	-0.004	0.000	*NA*	*NA*	0.000
Npas2	-1.236	-0.527	-0.859	-5.605	0.035	0.250	0.118	0.207	0.000	-0.182	0.000	0.000
Nr1d1	-17.238	-30.446	10.979	15.168	-0.291	0.100	0.192	0.049	0.000	0.000	0.000	0.000
Nr1d2	-51.031	-11.753	-0.415	-3.579	-0.085	0.179	0.201	0.093	0.000	0.000	0.000	0.360
Per1	-37.034	-14.077	-9.057	-12.196	-0.114	0.133	0.132	0.024	0.000	0.138	0.000	0.000
Per2	-27.580	-8.944	0.834	-21.464	0.103	0.268	0.457	0.144	0.000	0.000	0.000	0.000
Per3	-38.505	-10.182	2.242	-7.946	-0.077	0.377	0.485	0.288	0.000	0.000	0.000	0.607
Rora	-7.582	1.182	-2.238	-1.582	-0.076	0.046	-0.115	-0.039	0.000	0.000	0.239	0.000
Tef	-84.231	-28.625	-3.463	-13.690	-0.188	0.204	0.344	0.035	0.000	0.000	0.000	0.000
Decrease amplitude	14	10	11	12	10	0	2	5	3	1	0	0
Increase amplitude	2	6	5	4	6	16	14	11	2	3	1	3
No change in amplitude	0	0	0	0	0	0	0	0	11	11	14	13

Using the same CCGs from Table 2, we examined the phase order of CCGs. In circadian biology, the phase order is tightly regulated in transcription translation feedback loops. For example, *CLOCK* and *ARNT1* activate the expression of Per and Cry genes, which then upregulate proteins that inhibit their own transcription (Zhang et al., 2014). This crucial phase order is conserved between mouse and baboons, even when the exact phases of the genes are not (Mure et al., 2018). We assume this essential phase order is likely conserved between mice and humans within tissue and age.

To consider the cyclic properties of these data, we calculated the circular correlation coefficient between the CCG phases of mouse time course and CCG phases of either TOD or CHIRAL based analysis (Table 3). This reveals that using TOD leads to better coherence between mouse and human CCG phases. In Young, the average circular correlation was 0.57 using TOD and -0.26 using CHIRAL. In Old, the average circular correlation was 0.41 using TOD and -0.11 using CHIRAL. This negative correlation implies that CHIRAL has directional errors when reconstructing rhythmicity. Figure 3 shows each method's estimated CCG phase orders in Young muscle tissue.

Table 3: Circular correlation coefficients of CCG phase orders

Tissue	Age Group	Mouse vs. TOD	Mouse vs. CHIRAL
adrenal	young	0.774	-0.098
	old	-0.080	-0.540
heart	young	0.578	-0.424
	old	0.749	-0.414
lung	young	0.543	-0.668
	old	0.263	-0.235
muscle	young	0.405	0.148
	old	0.690	0.331

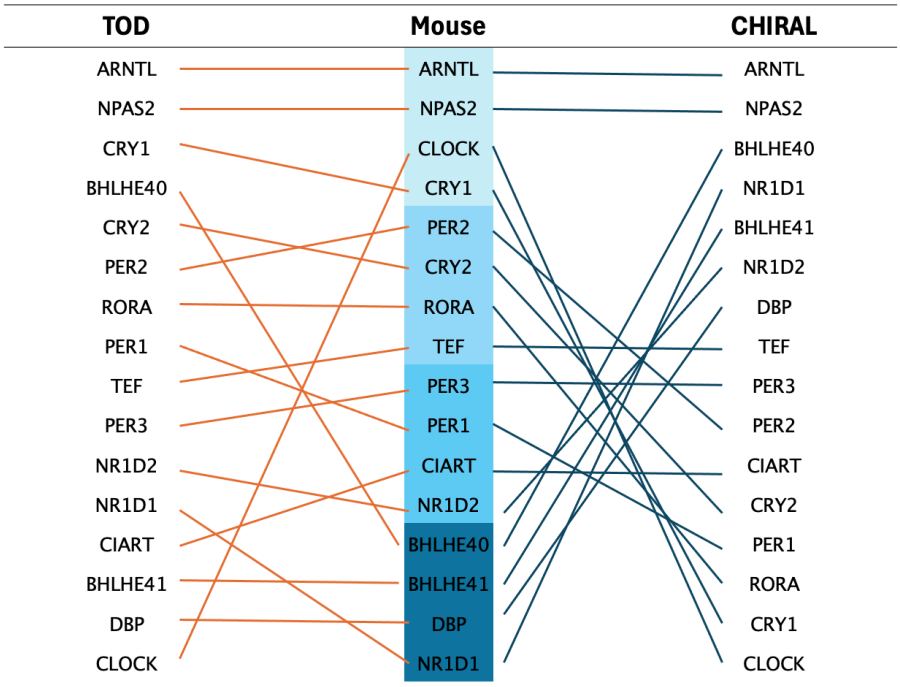

Figure 3: Phase orders of core clock genes across methods in Young lung tissue

3.3 Tissue specific analysis of age-related REGs

Given the moderately strong circular correlation of CCG phase orders for our rhythmicity results, we further examined the detected REGs within each tissue. First, the distributions of the peak phases of the REGs were explored (Figure 4). For nearly all tissues and ages, the peak phases display different distributions of two clusters. In lung and heart, the clusters shift forward by 2-3 hours with age (Figure 4A, 4C). In adrenal the clusters shift back 2-3 hours with age (Figure 4D). When the REGs are combined across all tissue in Figure 5, the peak phases in Old organize into two clusters between ZTs 19-5 and ZTs 8-16, suggesting peaks in anticipation of rest and active phases. This is a feature of rhythmicity in diurnal primates (Mure et al., 2014). However, in Young, the combined peak phases show a greater spread throughout the day. This could suggest that in Young, the rhythmicity patterns of each peripheral clock are more distinct.

The tissue and age-specific clusters of REG peak phases were then examined using Gene Ontology (GO)- based annotation for functional pathways.

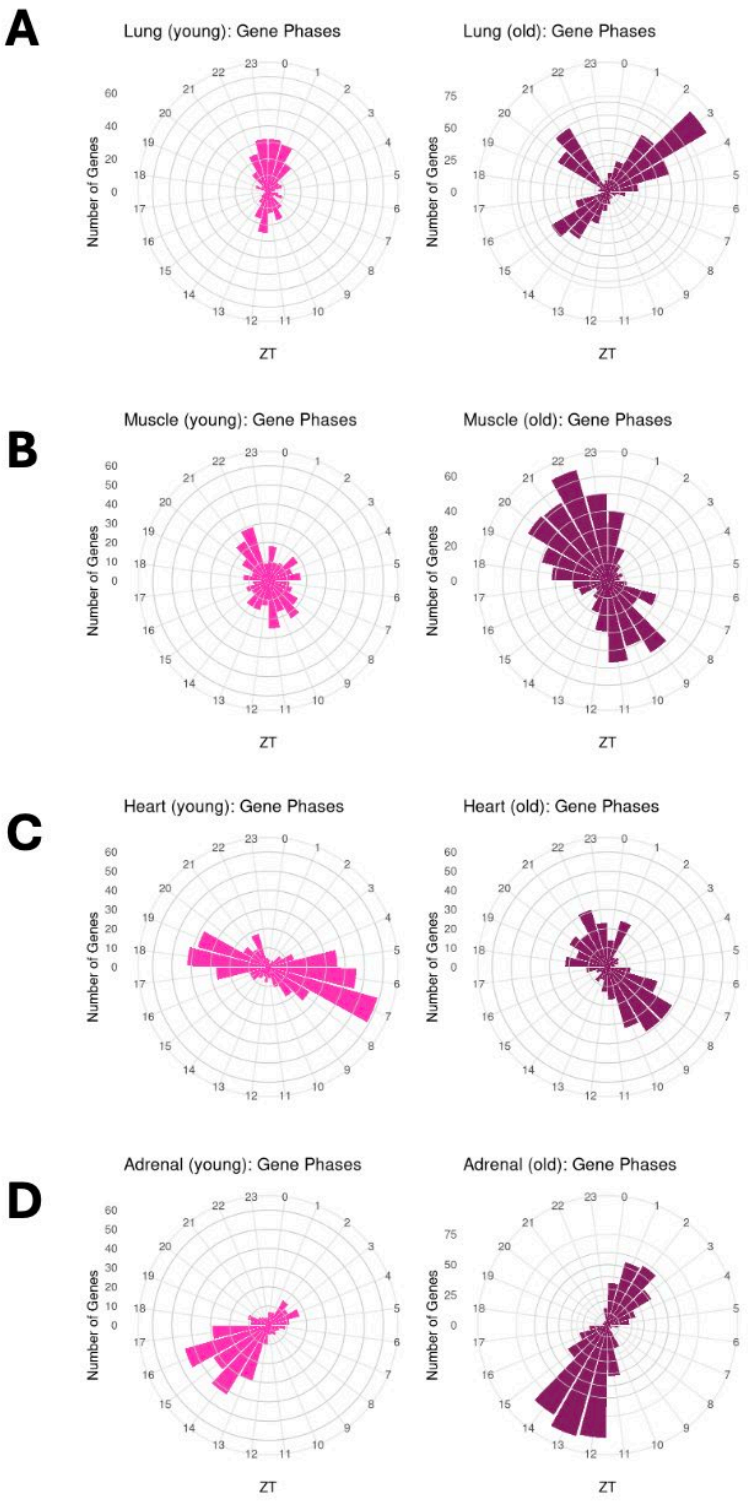

Figure 4: Radial plot of the distribution of estimated peak phases of the REGs from each tissue

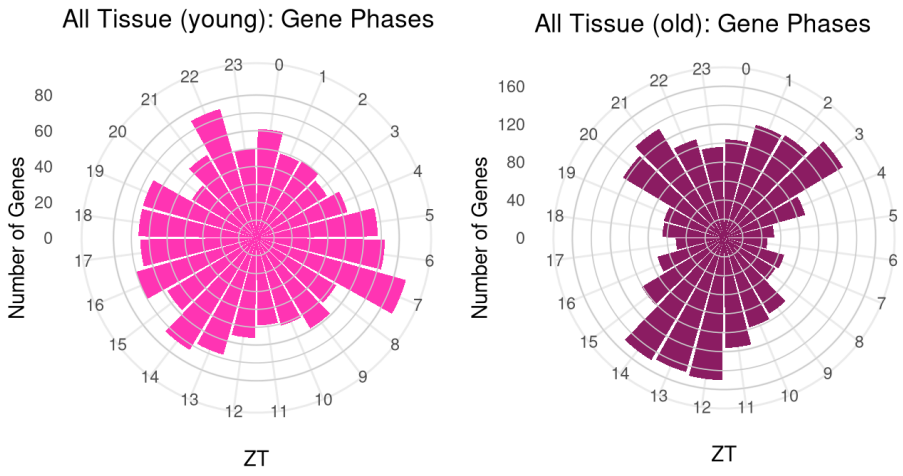

Figure 5: Radial plot of the distribution of estimated peak phases for all REGs combined across tissue

3.3.1 Pathway analysis of REGs identified in lung

Lungs are primarily known for facilitating gas exchange but are also crucial in the inflammatory response as the first line of defense against pathogenic microbes.

In our analysis (Table 4), we saw enrichment for fatty acid metabolism and inositol lipid signaling pathways in Young REGs. Alveoli are especially lipid rich and require fatty acids to maintain the integrity and fluidity of cellular membranes. Disruption of fatty acid synthesis affects the regeneration of alveolar epithelial cells and is implicated in pulmonary fibrosis and acute lung injury (Tian et al., 2023). Along the same lines, there is enrichment in maintenance of epithelial and mesenchymal cells in Young REGs. For example, autophagic processes in cardiac and mesenchymal cells maintain the function of pulmonary airways in the lung (Liao et al., 2019).

These pathways are not enriched in Old REGs. Rather, in Old, cluster ZT 19-22 includes pathways like cilium movement and xenobiotic metabolism. Both are involved in eliminating harmful substances in the environment and could be considered reactive functions.

Oxidative metabolic pathways and cellular respiration are enriched in Old but not Young at ZT0-6. This implies greater energy demands between the rest phase and active phase and will be a common pattern seen in the REGs of other tissues as well. Studies in mice have also found that the majority of cycling mitochondrial proteins peak during early light phase (corresponds to ZT0-6). The rate-limiting mitochondrial enzymes accumulate diurnally and are dependent on PER1/2. In PER1/2 knockout mice, the cycling of mitochondrial respiration is dampened (Neufield-Cohen et al., 2016).

It is curious to see mitochondrial respiration pathways only enriched in Old, as mitochondrial dysfunction is considered a hallmark of aging. One possible reason is that mammalian tissue shows inconsistencies in the rate of mitochondrial decline across the entire organism. For example, studies show a decline in mitochondrial respiration with age in human muscle, but not blood (Trounce et al., 1989; Ehinger et al., 2024). Similarly, in an animal study of 344 aging rats, there was no decline in respiration within platelets or heart tissue although changes were seen in skeletal muscle and kidney cortex (Jedlicka et al., 2022). In our analysis, we only see periodic activity of mitochondrial respiration in Old for lung, heart, and adrenal tissue, but not muscle. The tissue-specific rhythmicity of mitochondrial respiration could explain the tissue-specific stability of mitochondrial function with age.

Wolff et al. also saw apoptosis enriched in Young and cellular respiration enriched in Old. However, their main observation that immune-related pathways lost rhythmicity in the Old was not reflected in our analysis.

Table 4: GO pathways enriched by REGs that cycle in lung

Clusters refer to the distribution of REG peak phases in Figure 4A.

Age Group	Cluster (ZT)	Pathway	GeneRatio	P-Value	Q-Value
Young	7 - 14	positive regulation of fatty acid metabolic process	3/63	2.9e-04	1.2e-01
		gastrulation	5/63	5.3e-04	1.2e-01
		cardiac muscle cell apoptotic process	3/63	7.7e-04	1.2e-01
		regulation of cell-substrate adhesion	5/63	9.2e-04	1.2e-01
		mesenchymal cell apoptotic process	2/63	1.2e-03	1.2e-01
		regulation of unsaturated fatty acid biosynthetic process	2/63	1.2e-03	1.2e-01
		protein complex oligomerization	5/63	1.5e-03	1.4e-01
	19 - 4	rhythmic process	11/112	2.2e-06	3.6e-03
		regulation of circadian rhythm	6/112	7.2e-05	4.0e-02
		inositol lipid-mediated signaling	6/112	6.9e-04	1.4e-01
Old	11 - 17	hippo signaling	5/131	1.4e-05	2.3e-02
		chromatin remodeling	12/131	2.7e-05	2.3e-02
		positive regulation of monocyte differentiation	3/131	3.9e-05	2.3e-02
		fat cell differentiation	9/131	6.2e-05	2.9e-02
		myoblast differentiation	6/131	1.3e-04	3.7e-02
	19 - 22	axoneme assembly	17/71	1.6e-24	1.3e-21
		microtubule-based movement	23/71	6.2e-21	1.7e-18
		cilium organization	21/71	9.4e-19	1.9e-16
		extracellular transport	4/71	2.4e-05	1.1e-03
		xenobiotic metabolic process	4/71	1.3e-03	4.8e-02
	0 - 6	cellular respiration	12/187	6.6e-06	2.5e-03
		protein neddylation	5/187	7.9e-06	2.5e-03
		mitochondrial electron transport, NADH to ubiquinone	6/187	1.2e-05	2.9e-03
		ribonucleoprotein complex biogenesis	15/187	9.5e-05	1.5e-02
		oxidative phosphorylation	8/187	1.3e-04	1.7e-02
		nucleotide biosynthetic process	11/187	2.0e-04	1.9e-02
		iron-sulfur cluster assembly	4/187	2.2e-04	1.9e-02
		endoplasmic reticulum to Golgi vesicle-mediated transport	7/187	3.6e-04	2.4e-02

3.3.2 Pathway analysis of REGs identified in heart

As mentioned in the lung section, heart REGs in Old show enrichment in respiration pathways which is not seen in Young. Unlike in lung, this process peaks at ZT5-13, which corresponds to the active phase. Heart REGs in Young also show enrichment in heart valve morphogenesis and epithelial to mesenchymal transition (EMT). EMT serves as the basis for wound healing (Dongre et al., 2019). This supports the pattern found in lung REGs that rhythms of cell differentiation, growth, and maintenance more pronounced in Young.

Within REGs in both Young and Old, there is enrichment of the adaptive immune response and interferon signaling. This occurs at similar times- ZTs 14-23 in Young and ZTs 16-2 in Old. Adaptive immune responses are known to be regulated by the circadian clock, with enhanced immune reactivity occurring between the rest and active phases (Ince et al., 2023). Our analysis is consistent with this. Additionally, the continued rhythmicity of immune-related pathways is consistent with Wolff et al.'s finding that unlike other tissues, REG pathways in the heart are largely conserved across age.

Table 5: GO pathways enriched by REGs that cycle in heart

Clusters refer to the distribution of REG peak phases in Figure 4C.

Age Group	Cluster (ZT)	Pathway	GeneRatio	P-Value	Q-Value
Young	14 - 23	heart valve morphogenesis	5/137	7.9e-05	7.2e-02
		epithelial to mesenchymal transition	7/137	2.9e-04	7.6e-02
		positive regulation of immune effector process	8/137	8.2e-04	1.5e-01
		protein export from nucleus	4/137	9.3e-04	1.5e-01
		positive regulation of histone acetylation	3/137	1.4e-03	1.7e-01
		positive regulation of adaptive immune response	5/137	2.2e-03	1.7e-01
		C21-steroid hormone metabolic process	3/137	2.5e-03	1.7e-01
	2 - 11	regulation of IRE1-mediated unfolded protein response	3/178	2.9e-04	2.2e-01
		endosome to plasma membrane protein transport	3/178	5.3e-04	2.2e-01
		protein targeting to peroxisome	3/178	8.7e-04	2.2e-01
Old	5 - 13	mitochondrial respiratory chain complex assembly	12/135	7.0e-12	1.2e-08
		oxidative phosphorylation	11/135	1.1e-08	4.4e-06
		cellular respiration	12/135	2.1e-07	3.5e-05
		energy derivation by oxidation of organic compounds	13/135	1.1e-06	1.3e-04
	16 - 2	response to virus	16/146	1.4e-07	8.8e-05
		interferon-mediated signaling pathway	7/146	1.4e-05	3.3e-03
		protein localization to nucleus	11/146	2.9e-05	5.0e-03
		establishment of RNA localization	8/146	4.4e-05	5.0e-03
		rhythmic process	10/146	1.4e-04	1.4e-02
		circadian rhythm	8/146	2.3e-04	2.0e-02

3.3.3 Pathway analysis of REGs identified in muscle

This analysis found no overlap in the rhythmic processes across age in muscle. Following the trend in lung and heart, the most significantly enriched pathway in the REGs of Young muscle is cell morphogenesis. In Old, enriched pathways consisted of protein folding, p53 signal transduction, and NF-kappaB activity. The purpose of these processes is to maintain homeostasis against diverse stressors: unfolded proteins, DNA damage, and pathogens. They are each known to regulate the circadian clock. For example, p53 blocks BMAL1/CLOCK binding to the *Per2* promoter resulting in repressed *Per2* expression, and NF-kappaB binds to and represses BMAL1 at the same domain as CRY1 (Miki et al., 2014; Shen et al., 2021).

The enrichment of these pathways may be associated with our observation of more robust CCG rhythms with age. Wolff et al., who found less robust CCG rhythms with age, observed that the p53 and NF-kappaB pathways lost rhythmicity with age in muscle, heart, and lung.

Table 6: GO pathways enriched in REGs that cycle in muscle

Clusters refer to the distribution of REG peak phases in Figure 4B.

Age Group	Cluster (ZT)	Pathway	GeneRatio	P-Value	Q-Value
Young	7 - 15	base-excision repair	5/114	6.3e-06	1.2e-02
		steroid biosynthetic process	7/114	1.0e-04	1.0e-01
	19 - 1	regulation of cell morphogenesis	8/90	2.5e-05	4.2e-02
Old	6 - 14	protein-containing complex disassembly	10/205	3.4e-04	1.0e-01
		positive regulation of NF-kappaB transcription factor activity	8/205	3.9e-04	1.0e-01
		positive regulation of cell projection organization	12/205	5.7e-04	1.2e-01
		regulation of DNA-binding transcription factor activity	14/205	6.7e-04	1.2e-01
		signal transduction by p53 class mediator	8/205	6.8e-04	1.2e-01
		neurotrophin signaling pathway	4/205	7.1e-04	1.2e-01
		protein folding	8/205	3.1e-03	2.6e-01
	15 - 2	regulation of GTPase activity	18/273	7.7e-06	1.9e-02
		vascular process in circulatory system	14/273	3.9e-05	3.4e-02
		rhythmic process	15/273	4.4e-05	3.4e-02

3.3.4 Pathway analysis of REGs identified in adrenal medulla

The adrenal medulla releases catecholamine hormones like epinephrine and norepinephrine which regulate the autonomous nervous system. Important features of the adrenal medulla include innervation by preganglionic neurons for communicating with the body, and chromaffin cells which secrete neurohormones into the blood supply (Hofmann et al., 1981). Given the established circadian rhythms of norepinephrine and epinephrine (Linsell et al., 1985), it is unsurprising that the adrenal medulla would display REGs related to nervous system function. In this analysis (Table 7), we specifically see rhythms in synaptic assembly and chemical-synaptic signaling in Young. In Old, there is enrichment in neuron projection and axonogenesis. These pathways were not enriched in Wolff et al.'s adrenal gland results, possibly because they homogenized both adrenal cortex and medulla tissue. GTEx kept the two tissues distinct. However, Wolff et al.'s hypothalamus results did see rhythms in neuron development and projection in Old but not Young.

In Old, there is enrichment in metabolic pathways, including TOR signaling, fatty acid catabolism, and ribonucleotide metabolism. This suggests greater provision of energy occurs at ZT 9-18, between rest phase and activity onset, which is like Old REGs in the lung. In Old, there is rhythmicity in protein quality control not seen in Young. This was also observed in muscle. Wolff et al. found in their analysis that unfolded protein response pathways were generally maintained across age.

Table 7: GO pathways enriched in REGs that cycle in adrenal medulla

Clusters refer to the distribution of REG peak phases in Figure 4D.

Age Group	Cluster (ZT)	Pathway	GeneRatio	P-Value	Q-Value
Young	23 - 7	cell junction assembly	11/69	6.6e-07	1.0e-03
		synapse assembly	7/69	8.3e-06	4.6e-03
		modulation of chemical synaptic transmission	10/69	1.2e-05	4.6e-03
		regulation of trans-synaptic signaling	10/69	1.2e-05	4.6e-03
		positive regulation of cell projection organization	7/69	3.3e-04	4.2e-02
		adaptive thermogenesis	5/69	3.3e-04	4.2e-02
	11 - 20	No enriched pathways	-	-	-
Old	22 - 6	regulation of neuron projection development	18/209	3.7e-06	8.5e-03
		axonogenesis	16/209	2.7e-05	1.4e-02
		cell junction assembly	15/209	1.6e-04	5.5e-02
	9 - 18	monocarboxylic acid catabolic process	9/247	6.4e-05	9.9e-02
		protein quality control for misfolded or incompletely synthesized proteins	4/247	4.8e-04	1.1e-01
		ribonucleotide metabolic process	16/247	5.0e-04	1.1e-01
		fatty acid catabolic process	7/247	5.0e-04	1.1e-01
		regulation of TOR signaling	7/247	9.1e-04	1.4e-01

3.4 Age-associated differential expression analysis within time domains

In addition to detecting rhythmic genes, Wolff et al. divided their time course data over four time domains and examined temporal differences in age-related changes in genes expression. We did a similar analysis with the goal of seeing how translatable Wolff et al.'s mouse results were to humans. The tissue samples were binned into four time domains based on donor's TOD: the active phase, activity offset, rest phase, and activity onset. We performed differential expression analysis to define time domain specific genes that were upregulated or downregulated with age.

Differentially expressed genes (DEGs) were defined by a cutoff of q-value < 0.1 (Figure 6). Similar to Wolff et al.'s result, the large majority of identified DEGs were time domain specific within tissues, and tissue specific within time domains. The most DEGs identified was in lung tissue, with an average of 1696 DEGs identified in each of the four time domain. The least number of DEGs identified was in heart tissue with an average of 41 DEGs identified in each time domain. This was also found in Wolff et al.'s results and supported their conclusion that heart tissue shows the least change in age.

Our differential expression genes were compared to Wolff et al.'s results using a rank-rank-hypergeometric-overlap (RRHO). This method allowed us to identify concordant and discordant differential patterns between mice and humans within each tissue and time domain. Muscle, lung, and heart tissue were included for this analysis. Adrenal was excluded because Wolff et al. did not provide the DE results for this tissue.

High concordance was seen in lung tissue (Figure 7). Except for rest phase, most of the genes that significantly overlapped between mice and human were either upregulated in both or downregulated in both. Muscle and heart tissues either saw few significantly overlapped genes or

saw discordant patterns. This implies that only in lung tissue do mice and humans share age-related changes at the same time domains. Wolff et al. expressed that the potential application for their DE analysis is to target therapeutics more precisely. Given the RRHO results, these time-of-day molecular mappings require a species-specific perspective.

Table 8 shows pathway enriched in the concordant genes identified in lung tissue. The goal is to provide supporting evidence to the lung REG analysis, because certain pathways found rhythmic in humans were not rhythmic in mouse, or vice versa. For example, Wolff et al. saw an age-related loss in rhythmicity of genes related to the immune system. However, they also found in their DE analysis, that there is an upregulation of immune-related genes with age, specifically in the active and activity offset phase. They suggest that this time-of-day specific upregulation is to compensate for loss of rhythmicity in Young. Similarly, although our analysis did not identify any rhythmic pathways related to immune function, we do see that upregulation in immune-related DEGs, also in active and activity offset phases.

Consistent with the lung rhythmicity patterns, the lung DEGs in both human and mouse show downregulation in epithelial cell proliferation and an upregulation in cellular respiration at activity onset. Within the active phase, there is concordant upregulation in cilium organization. It is known that lack of proliferation in aging broncoepitheial cells impairs mucous clearance (Brandenburger et al., 2016). Upregulation of cilium activity could be a reactive response to this. Lastly, throughout the day, there is concordant downregulation of stress response pathways related to endoplasmic reticulum stress and oxidative stress.

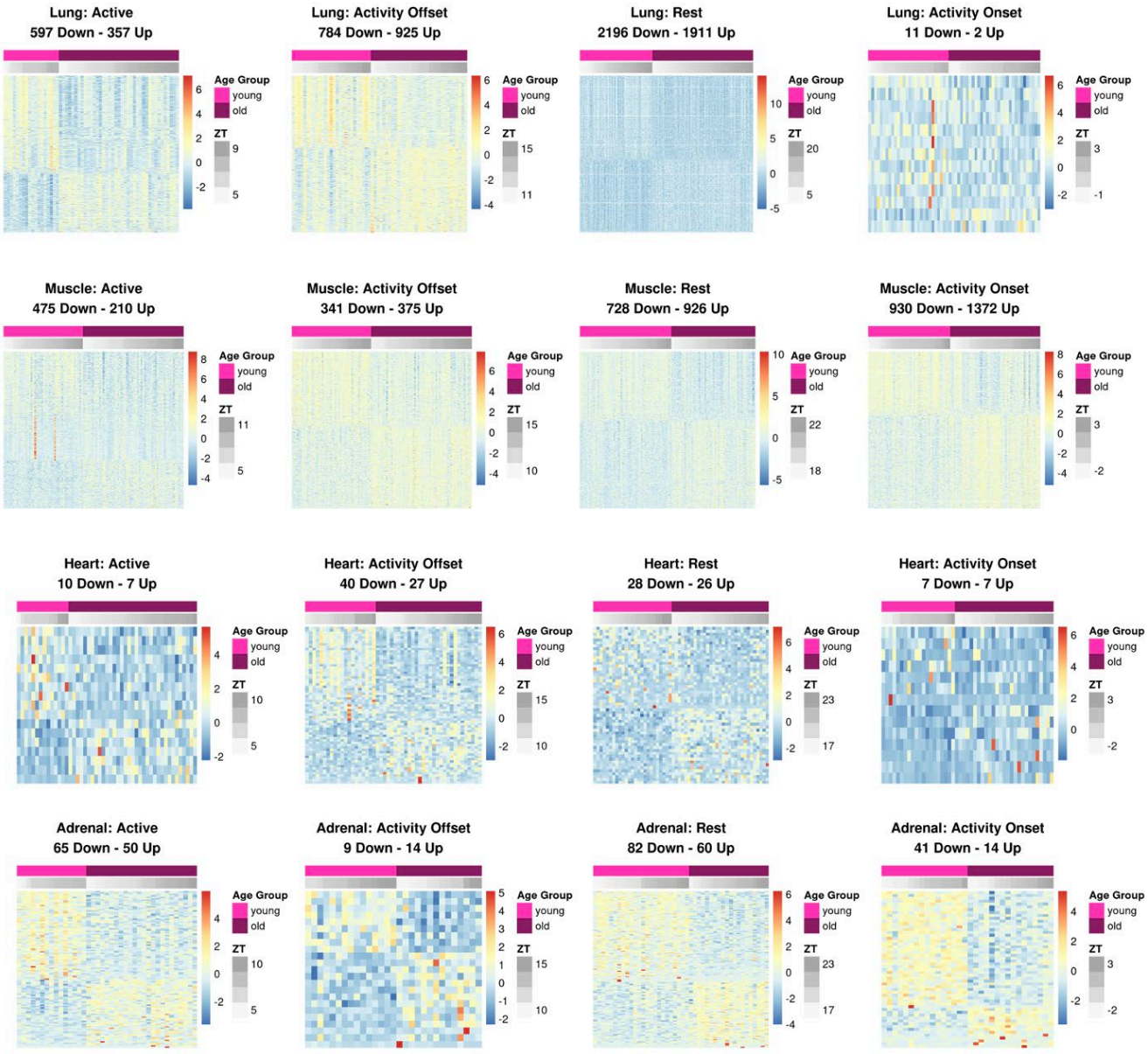

Figure 6: Heatmap of age-associated DEGs identified within time domains

Heatmap displays Z-scores of log2fold change.

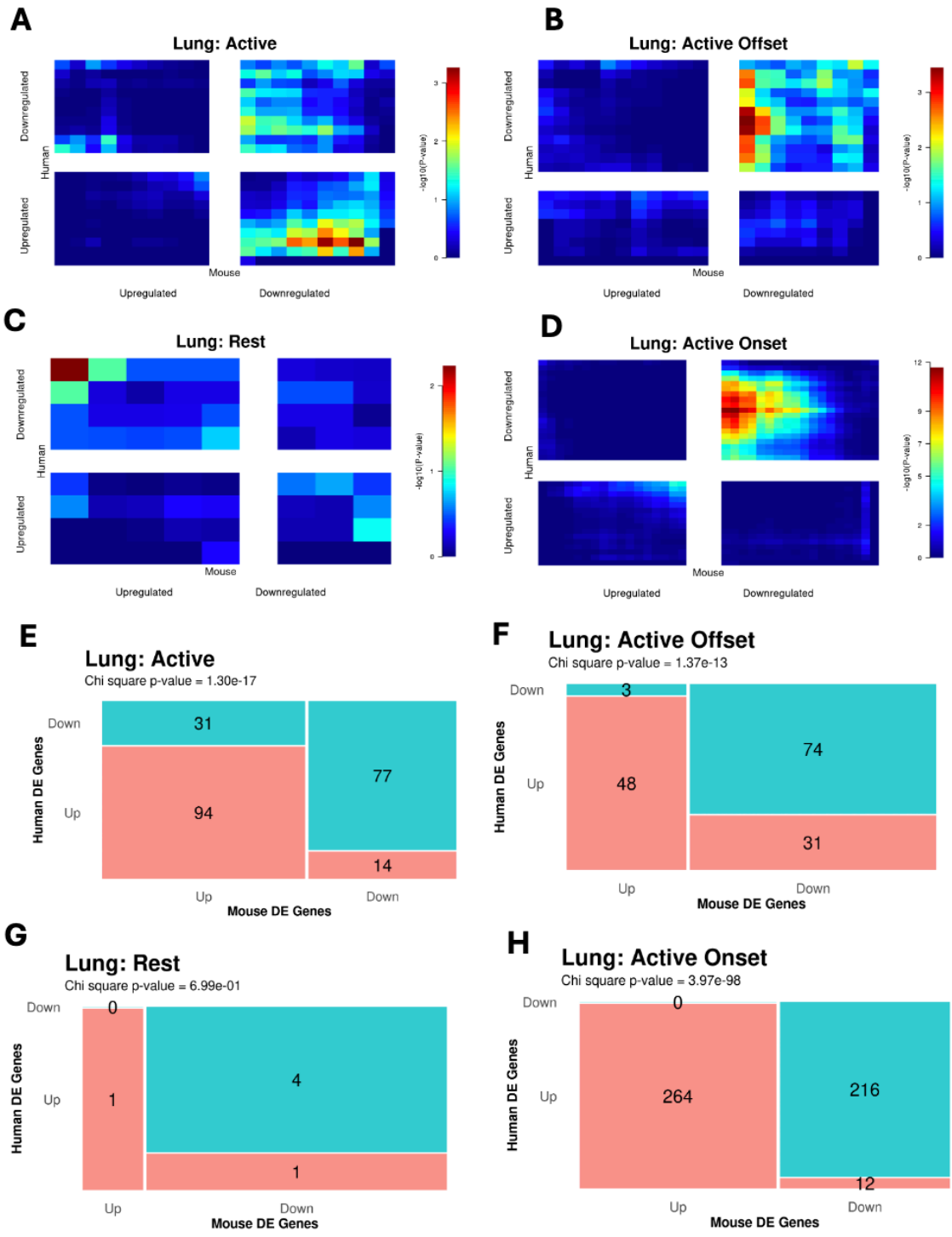

Figure 7: RRHO between mouse and human lung gene sets

A-D depict heatmaps of the -log10(P-values) between overlapping genes. E-H depict the number of overlapping genes found signficant in each condition.

Table 8: GO pathways enriched in DEGs that are concordant between mouse and human lung tissue

Time Domain	Direction with Age	Pathway	GeneRatio	P-Value	Q-Value
Active	Downregulated	positive regulation of response to endoplasmic reticulum stress	3/77	1.2e-04	3.3e-02
		rRNA processing	5/77	2.8e-04	3.3e-02
		regulation of proteolysis involved in protein catabolic process	5/77	3.6e-04	3.3e-02
	Upregulated	cilium organization	13/94	9.0e-10	1.7e-07
		respiratory system development	6/94	2.7e-04	1.8e-02
		regulation of innate immune response	6/94	1.7e-03	3.3e-02
Active Offset	Downregulated	ribonucleoprotein complex biogenesis	7/69	6.9e-05	5.3e-02
		histone H3 deacetylation	2/69	3.7e-04	1.1e-01
		ncRNA processing	6/69	4.3e-04	1.1e-01
	Upregulated	T cell proliferation	5/48	5.4e-05	7.3e-03
		carbohydrate derivative catabolic process	4/48	1.5e-04	1.5e-02
		regulation of G1/S transition of mitotic cell cycle	4/48	1.8e-04	1.5e-02
Rest	Downregulated	No enriched pathways	-	-	-
	Upregulated	No enriched pathways	-	-	-
Active Onset	Downregulated	protein autophosphorylation	12/212	2.9e-07	5.5e-04
		regulation of epithelial cell proliferation	13/212	2.0e-05	2.5e-03
		cell death in response to oxidative stress	6/212	1.1e-04	4.9e-03
	Upregulated	muscle cell development	20/247	2.3e-14	4.8e-11
		mitochondrial translation	12/247	1.9e-09	3.5e-07
		cellular respiration	11/247	1.4e-05	5.5e-04

4.0 Discussion

Several rhythmic characteristics and pathways were found similar between Wolff et al.'s results and ours. With age, the peak phases of genes tend to distribute into two clusters at active onset and active offset times. This could imply that in Young, there is a greater diversity in the timing of the daily transcriptional program. On the other hand, in Old, the clusters of peak phases could be reactive to stressors occurring during these times.

Across all tissues, we notice trends in two biological processes. In Young, there tends to be rhythmicity in cell growth, differentiation, and tissue development. These pathways are seen less in Old. In Old, we see rhythmicity in cellular respiration and oxidative phosphorylation, which is not seen in Young. This observation meshes well with the peak phase clustering information. In Young, there is a focus on maintaining cell and tissue integrity throughout the day. In Old, energy demands during the transitions between rest and active phase are associated with peaks in REGs.

These results contribute to existing knowledge on aging. A main feature of aging is increased cellular senescence, a state of irreversible growth cycle arrest. Senescence is accompanied by impaired cellular function. Most notably, mitochondrial dysfunction is both a cause and a consequence of senescence. In our analysis, the senescence phenotype likely presents as age-associated loss of rhythmicity and gene expression of cell growth and differentiation pathways.

On the other hand, it is unclear how the mitochondrial dysfunction phenotype relates to our observed age-associated and time-dependent increases in cellular respiration related rhythmicity and gene expression. One possibility is Wolff et al.'s hypothesis of compensatory reactive pathways with age: mitochondrial dysfunction in the old creates time-of day specific vulnerability,

which is overcome by upregulation of response genes. Previous studies have also found evidence of transcriptional upregulation of mitochondrial genes in response to dysfunctional mitochondrial biogenesis (Celotto et al., 2011; Bergen et al., 2011; Chen et al., 2022). A second possibility is that rhythmicity with age is protective: sustained rhythmicity of mitochondrial respiration genes with age in certain tissues contributes to why mitochondrial function declines with age in certain tissues but not others (Ehinger et al., 2024). A third possibility is that 24-hour oscillations in the old is itself a symptom of dysfunction. Besides 24-hour rhythms, there also exist ultradian rhythms, which oscillate with periods less than 24 hours. 8–12-week-old mice (corresponds to 35-40 human years) exhibit 12-hr oscillations in mitochondria-associated metabolism pathway (Zhu et al., 2018). Additionally, certain ultradian rhythms lengthen in period during disease and aging (Lopp et al., 2017; Scott et al., 2023) Our analysis was limited to a 24-hour period and cannot detect changes in oscillatory period with age.

In this discussion, we only emphasize the enriched biological processes that exhibited a consistent trend across all tissues. Interpretation of our other results is complicated by the reduced rhythmicity of CCGs in some Young tissues. It is established that CCGs are more robust in the younger organisms. If a pathway was not found rhythmic in certain Young tissues, it may be because of study limitations rather than biological truth.

Several factors may contribute to the lack of REGs detected in Young. According to the cohort demographics, the Young group had smaller sample sizes. The Young group also had wider age distributions with a standard deviation of 7-8 years compared to 3 years in Old. This may have contributed to greater heterogeneity within the Young groups, and difficulty in reconstructing rhythmicity.

Another obstacle in detecting rhythmic genes was the use of TOD to order donors. We introduced Talamanca et al.'s analysis because they similarly used GTEx data to investigate age-associated circadian changes, but also incorporated CHIRAL, an algorithm for estimating donor phase. CHIRAL did improve Talamanca et al.'s ability to detect REGs. Compared to our analysis, there is less difference in the number of REGs detected between Young and Old. Talamanca et al. also described a stable amplitude for most CCGs with age.

Our main concern with the CHIRAL-based analysis is its inaccuracies in estimating the phase order of CCGs. This would be problematic if someone is interested in the mechanisms and causal relationships between specific REGs. On the other hand, the phase orders in our analysis were consistent with Wolff et al.'s. However, a confounding factor is that our analysis and Wolff et al.'s both detected rhythmicity using the Cosinor model, whereas Talamanca et al. employed a multivariate harmonic regression model, described in Methods. While the Cosinor model only fits univariate data to a single periodic component, a multivariate harmonic regression accommodates multiple variables and periodic components.

Overall, our findings present multiple avenues for future research. It would be meaningful to extend this analysis with more tissue types, a greater range of periods, and narrower continuous age intervals. This would enhance the systems-level goal of the study. Phase estimation algorithms can be implemented. Specifically, the phase order estimation of CHIRAL could be refined using age-specific and tissue-specific clock references, and order-restricted inference methods (Larriba et al., 2022). Moreover, conducting functional assays is crucial to decipher the underlying biological mechanisms tied to our findings and to investigate potential interventions for promoting healthy aging.

Bibliography

Cahill, K. M., Huo, Z., Tseng, G. C., Logan, R. W., & Seney, M. L. (2018). Improved identification of concordant and discordant gene expression signatures using an updated rank-rank hypergeometric overlap approach. Scientific Reports, 8(1). https://doi.org/10.1038/s41598-018-27903-2

Celotto, A. M., Chiu, W. K., van Voorhies, W., & Palladino, M. J. (2011). Modes of metabolic compensation during mitochondrial disease using the drosophila model of ATP6 dysfunction. PLoS ONE, 6(10). https://doi.org/10.1371/journal.pone.0025823

Chen, C. Y., Logan, R. W., Ma, T., Lewis, D. A., Tseng, G. C., Sibille, E., & McClung, C. A. (2016). Effects of aging on circadian patterns of gene expression in the human prefrontal cortex. Proceedings of the National Academy of Sciences of the United States of America, 113(1). https://doi.org/10.1073/pnas.1508249112

Chen, X., Lin, H., Xiong, W., Pan, J., Huang, S., Xu, S., He, S., Lei, M., Yu Chang, A. C., & Zhang, H. (2022). p53-Dependent Mitochondrial Compensation in Heart Failure With Preserved Ejection Fraction. Journal of the American Heart Association, 11(11). https://doi.org/10.1161/JAHA.121.024582

Cornelissen, G. (2014). Cosinor-based rhythmometry. In Theoretical Biology and Medical Modelling (Vol. 11, Issue 1). https://doi.org/10.1186/1742-4682-11-16

Cox, K. H., & Takahashi, J. S. (2019). Circadian clock genes and the transcriptional architecture of the clock mechanism. Journal of Molecular Endocrinology, 63(4). https://doi.org/10.1530/JME-19-0153

Dongre, A., & Weinberg, R. A. (2019). New insights into the mechanisms of epithelial–mesenchymal transition and implications for cancer. In Nature Reviews Molecular Cell Biology (Vol. 20, Issue 2). https://doi.org/10.1038/s41580-018-0080-4

Farajnia, S., Michel, S., Deboer, T., van der Leest, H. T., Houben, T., Rohling, J. H. T., Ramkisoensing, A., Yasenkov, R., & Meijer, J. H. (2012). Evidence for neuronal desynchrony in the aged suprachiasmatic nucleus clock. Journal of Neuroscience, 32(17). https://doi.org/10.1523/JNEUROSCI.0469-12.2012

Hofmann, F. (1981). Metabolic and endocrine physiology, 4th edn. Molecular and Cellular Endocrinology, 21(3). https://doi.org/10.1016/0303-7207(81)90020-4

Hood, S., & Amir, S. (2017). The aging clock: Circadian rhythms and later life. In Journal of Clinical Investigation (Vol. 127, Issue 2). https://doi.org/10.1172/JCI90328

Hu, K., van Someren, E. J. W., Shea, S. A., & Scheer, F. A. J. L. (2009). Reduction of scale invariance of activity fluctuations with aging and Alzheimer's disease: Involvement of the circadian pacemaker. Proceedings of the National Academy of Sciences of the United States of America, 106(8). https://doi.org/10.1073/pnas.0806087106

Inokawa, H., Umemura, Y., Shimba, A., Kawakami, E., Koike, N., Tsuchiya, Y., Ohashi, M., Minami, Y., Cui, G., Asahi, T., Ono, R., Sasawaki, Y., Konishi, E., Yoo, S. H., Chen, Z., Teramukai, S., Ikuta, K., & Yagita, K. (2020). Chronic circadian misalignment accelerates immune senescence and abbreviates lifespan in mice. Scientific Reports, 10(1). https://doi.org/10.1038/s41598-020-59541-y

Jedlička, J., Tůma, Z., Razak, K., Kunc, R., Kala, A., Peña, S. P., Lerchner, T., Ježek, K., & Kuncová, J. (2022). Impact of Aging on Mitochondrial Respiration in Various Organs. Physiological Research, 71. https://doi.org/10.33549/physiolres.934995

Larriba, Y., Rueda, C., Fernández, M. A., & Peddada, S. D. (2020). Order restricted inference in chronobiology. Statistics in Medicine, 39(3). https://doi.org/10.1002/sim.8397

Li, J. Z., Bunney, B. G., Meng, F., Hagenauer, M. H., Walsh, D. M., Vawter, M. P., Evans, S. J., Choudary, P. v., Cartagena, P., Barchas, J. D., Schatzberg, A. F., Jones, E. G., Myers, R. M., Watson, S. J., Akil, H., & Bunney, W. E. (2013). Circadian patterns of gene expression in the human brain and disruption in major depressive disorder. Proceedings of the National Academy of Sciences of the United States of America, 110(24). https://doi.org/10.1073/pnas.1305814110

Liao, S. X., Sun, P. P., Gu, Y. H., Rao, X. M., Zhang, L. Y., & Ou-Yang, Y. (2019). Autophagy and pulmonary disease. In Therapeutic Advances in Respiratory Disease (Vol. 13). https://doi.org/10.1177/1753466619890538

Linsell, C. R., Lightman, S. L., Mullen, P. E., Brown, M. J., & Causon, R. C. (1985). Circadian rhythms of epinephrine and norepinephrine in man. Journal of Clinical Endocrinology and Metabolism, 60(6). https://doi.org/10.1210/jcem-60-6-1210

Miki, T., Matsumoto, T., Zhao, Z., & Lee, C. C. (2013). P53 regulates Period2 expression and the circadian clock. Nature Communications, 4. https://doi.org/10.1038/ncomms3444

Moore-Ede, M. C. (1986). Physiology of the circadian timing system: Predictive versus reactive homeostasis. American Journal of Physiology - Regulatory Integrative and Comparative Physiology, 250(5 (19/5)). https://doi.org/10.1152/ajpregu.1986.250.5.r737

Mure, L. S., Le, H. D., Benegiamo, G., Chang, M. W., Rios, L., Jillani, N., Ngotho, M., Kariuki, T., Dkhissi-Benyahya, O., Cooper, H. M., & Panda, S. (2018). Diurnal transcriptome atlas of a primate across major neural and peripheral tissues. Science, 359(6381). https://doi.org/10.1126/science.aao0318

Neufeld-Cohen, A., Robles, M. S., Aviram, R., Manella, G., Adamovich, Y., Ladeuix, B., Nir, D., Rousso-Noori, L., Kuperman, Y., Golik, M., Mann, M., & Asher, G. (2016). Circadian control of oscillations in mitochondrial rate-limiting enzymes and nutrient utilization by

PERIOD proteins. Proceedings of the National Academy of Sciences of the United States of America, 113(12). https://doi.org/10.1073/pnas.1519650113

NIH. (2010, October 7). NIH launches Genotype-Tissue Expression project. NIH News Releases.

Reinberg, A., & Ashkenazi, I. (2003). Concepts in human biological rhythms. In Dialogues in Clinical Neuroscience (Vol. 5, Issue 4). https://doi.org/10.31887/dcns.2003.5.4/areinberg

Roenneberg, T., Kuehnle, T., Juda, M., Kantermann, T., Allebrandt, K., Gordijn, M., & Merrow, M. (2007). Epidemiology of the human circadian clock. In Sleep Medicine Reviews (Vol. 11, Issue 6). https://doi.org/10.1016/j.smrv.2007.07.005

Scott, M. R., Zong, W., Ketchesin, K. D., Seney, M. L., Tseng, G. C., Zhu, B., & McClung, C. A. (2023). Twelve-hour rhythms in transcript expression within the human dorsolateral prefrontal cortex are altered in schizophrenia. PLoS Biology, 21(1). https://doi.org/10.1371/journal.pbio.3001688

Shen, Y., Endale, M., Wang, W., Morris, A. R., Francey, L. J., Harold, R. L., Hammers, D. W., Huo, Z., Partch, C. L., Hogenesch, J. B., Wu, Z. H., & Liu, A. C. (2021). NF-κB modifies the mammalian circadian clock through interaction with the core clock protein BMAL1. PLoS Genetics, 17(11). https://doi.org/10.1371/journal.pgen.1009933

Takahashi, J. S. (2017). Transcriptional architecture of the mammalian circadian clock. In Nature Reviews Genetics (Vol. 18, Issue 3). https://doi.org/10.1038/nrg.2016.150

Tian, Y., Duan, C., Feng, J., Liao, J., Yang, Y., & Sun, W. (2023). Roles of lipid metabolism and its regulatory mechanism in idiopathic pulmonary fibrosis: A review. International Journal of Biochemistry and Cell Biology, 155. https://doi.org/10.1016/j.biocel.2022.106361

Trounce, I., Byrne, E., & Marzuki, S. (1989). DECLINE IN SKELETAL MUSCLE MITOCHONDRIAL RESPIRATORY CHAIN FUNCTION: POSSIBLE FACTOR IN AGEING. The Lancet, 333(8639). https://doi.org/10.1016/S0140-6736(89)92143-0

Van Bergen, N. J., Crowston, J. G., Kearns, L. S., Staffieri, S. E., Hewitt, A. W., Cohn, A. C., Mackey, D. A., & Trounce, I. A. (2011). Mitochondrial oxidative phosphorylation compensation may preserve vision in patients with OPA1-linked autosomal dominant optic atrophy. PLoS ONE, 6(6). https://doi.org/10.1371/journal.pone.0021347

Xue, X., Zong, W., Huo, Z., Ketchesin, K. D., Scott, M. R., Petersen, K. A., Logan, R. W., Seney, M. L., McClung, C., & Tseng, G. (2023). DiffCircaPipeline: a framework for multifaceted characterization of differential rhythmicity. Bioinformatics, 39(1). https://doi.org/10.1093/bioinformatics/btad039

Zhang, R., Lahens, N. F., Ballance, H. I., Hughes, M. E., & Hogenesch, J. B. (2014). A circadian gene expression atlas in mammals: Implications for biology and medicine. Proceedings of the National Academy of Sciences of the United States of America, 111(45). https://doi.org/10.1073/pnas.1408886111

Zhu, B., Dacso, C. C., & O'Malley, B. W. (2018). Unveiling "Musica Universalis" of the cell: A brief history of biological 12-hour rhythms. Journal of the Endocrine Society, 2(7). https://doi.org/10.1210/JS.2018-00113

Zhu, Y., Wang, L., Yin, Y., & Yang, E. (2017). Systematic analysis of gene expression patterns associated with postmortem interval in human tissues. Scientific Reports, 7(1). https://doi.org/10.1038/s41598-017-05882-0